Electronic properties of triangular and hexagonal MoS_2 quantum dots

S. Pavlović* and F. M. Peeters†

Departement Fysica, Universiteit Antwerpen Groenenborgerlaan 171, B-2020 Antwerpen, Belgium

(Received 30 January 2015; revised manuscript received 9 March 2015; published 10 April 2015)

Using the tight-binding approach, we calculate the electronic structure of triangular and hexagonal MoS_2 quantum dots. Due to the orbital asymmetry we show that it is possible to form quantum dots with the same shape but having different electronic properties. The electronic states of triangular and hexagonal quantum dots are explored, as well as the local and total density of states and the convergence towards the bulk spectrum with dot size is investigated. Our calculations show that: (1) edge states appear in the band gap, (2) that there are a larger number of electronic states in the conduction band as compared to the valence band, and (3) the relative number of edge states decreases with increasing dot size.

DOI: 10.1103/PhysRevB.91.155410 PACS number(s): 73.22.−f

I. INTRODUCTION

Recently, two-dimensional atomic crystals have been fabricated with distinct properties. Molybdenium disulfide (MoS_2) belongs to the group-VIB transition metal dichalcogenides (TMDs) MX_2 (M = Mo, W; X = S, Se, T), a newly emerged member of the two-dimensional crystal family, which have recently gained significant attention due to their interesting electrical and optical properties. Most importantly is its direct band gap [1–5] in the visible frequency range and the excellent carrier mobility at room temperature [6–11], which makes them strong candidates for future electronic and optoelectronic applications.

Monolayer MoS_2 can be considered as a semiconductor analog of graphene, where, like in graphene, both the conduction and valence band edges are located at the two corners of the Brillouin zone, i.e., K and $-K$ points. This gives electrons and holes an extra valley degree of freedom which can be used for encoding information and subsequent processing [12–16]. Other interesting properties include valley dependent interband transitions: interband transitions in the K ($-K$) valley can only be excited by left- (right-)handed circular polarized light [13,17]. Using this selection rule, optical pumping of valley polarization, and optical generation of valley coherence, has been demonstrated [18]. Recently, it was shown that stacking layers of TMDs in a particular way creates bilayers with tunable band gap, making them strong candidates for usage in new optoelectronic devices [19]. Another important property of two-dimensional transition metal dichalcogenides is the strong coupling between spin and valley pseudospin. These quantum degrees of freedom can be controlled and a single electron in monolayer quantum dots might be used as an information carrier for quantum spintronics and/or valleytronic.

As a relatively new material, MoS_2 quantum dots have not yet been researched extensively. Some of the previous works on MoS_2 quantum dots includes their use as valley-spin filters, and their use as quantum bits. It was concluded that, due to the relatively strong intrinsic spin-orbit splitting in the conduction band, the most realistic option appears to be a combined spin-valley (Kramers) qubit at low magnetic fields [20]. In contrast to previous theoretical approaches where quantum dots were created by electronic gating [20] or by lateral heterostructuring with other TMDs [21], here we consider flakes, i.e., finite size MoS_2 monolayers, of different shape.

This paper is organized as follows. In Sec. II we present the tight-binding model that is applicable to MoS_2, as well as other TMDs. Then, in Sec. III, we discuss the consequences of the asymmetric orbitals in the Mo atom layer. In Sec. IV we calculate the electronic structure and density of states (DOS) of triangular quantum dots. A similar investigation for hexagonal quantum dots is presented in Sec. V and the effect of system size on the DOS is studied. Conclusions are given in the final section.

II. TIGHT-BINDING MODEL

Monolayer MoS_2 consists of a layer of Mo atoms sandwiched between two layers of S atoms. Both the Mo layer and the S layers form a trigonal lattice, with each Mo atom being connected with three S atoms in the upper layer and three S atoms in the lower layer. Thus, a monolayer of MoS_2 has the D_{3h} point group symmetry. Since the lattice is trigonal, each atom in a layer (either S or Mo) is coordinated up to six other atoms in the same layer, whose relative positions to it are given by the vectors $\mathbf{R}_1, \ldots, \mathbf{R}_6$, as shown in Fig. 1. Distance between atoms is equal to the lattice constant $a = 0.319$ nm.

From earlier theoretical studies [22,23] and first-principle investigations [24–27], it is known that Bloch states in monolayer MoS_2 near the band edges consist of Mo d orbitals, mainly d_{z^2},d_{xy}, and $d_{x^2-y^2}$ orbitals, while the contribution from s orbitals and p orbitals (from which the bond between Mo and S is formed) is small in these bands. Thus, for calculating the valence and conduction band states within the tight-binding method, a good approximation is to only consider nearest-neighbor hopping between the atoms in the Mo layer and to consider the hopping between these three d orbitals. Since d_{xy} and $d_{x^2-y^2}$ orbitals are asymmetric in the plane of the Mo atoms, the hopping between neighboring Mo atoms will depend on their relative positions. Since three orbitals contribute, the hopping between two atoms is described by a 3×3 matrix, whose elements are hopping integrals. If, for simplicity, we denote the orbitals as $|\phi_j\rangle$, where $j = 1,2,3$ with $\phi_1 = |d_{z^2}\rangle$, $\phi_2 = |d_{xy}\rangle$, and $\phi_3 = |d_{x^2-y^2}\rangle$, then the hopping

*stefan.pavlovic@uantwerpen.be
†francois.peeters@uantwerpen.be

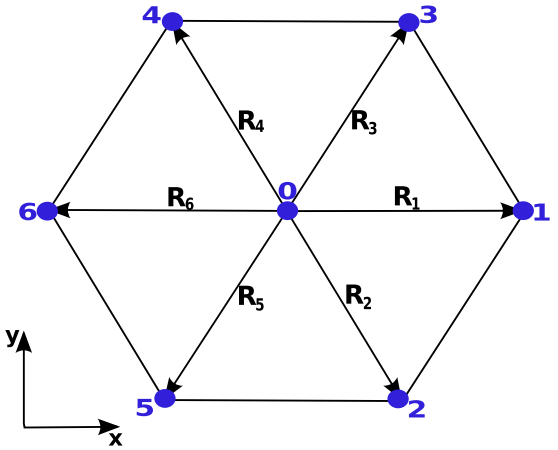

FIG. 1. (Color online) One atom in the lattice, like the atom denoted with number 0, is surrounded with up to six other atoms, denoted in the figure with numbers 1–6, whose relative positions to it are given with $\mathbf{R}_1,\ldots,\mathbf{R}_6$ vectors.

integrals between atoms whose relative position to one another is given by the vector $\mathbf{R}_n$ are obtained as

$$E_{jj'}(\mathbf{R}_n) = \langle\phi_j(\mathbf{r})|\hat{H}|\phi_{j'}(\mathbf{r}-\mathbf{R}_n)\rangle, \tag{1}$$

where $n = 1$–6.

However, instead of calculating the hopping integrals for every pair of atoms, we calculate the hopping integrals for one pair and obtain the rest in the following way:

$$E_j(\hat{g}_m\mathbf{R}_n) = D(\hat{g}_m)E_j(\mathbf{R}_n)D(\hat{g}_m)^\dagger, \tag{2}$$

where $E_j(\hat{g}_m\mathbf{R}_n) = [E_{j1}(\hat{g}_m\mathbf{R}_n)\,E_{j2}(\hat{g}_m\mathbf{R}_n)\,E_{j3}(\hat{g}_m\mathbf{R}_n)]^T$ and $D(\hat{g}_m)$ is a matrix representing symmetry operation $\hat{g}_m$ which transforms $\mathbf{R}_n$ to $\mathbf{R}_m$. Only a subset of symmetry operations of the D_{3h} symmetry group, $\{\hat{E},\hat{C}_3,\hat{C}_3^2,\hat{\sigma}_v,\hat{\sigma}_v',\hat{\sigma}_v''\}$, where $\hat{E}$ is the identity operation, $\hat{C}_3$ rotation by $2\pi/3$ around the z axis, and σ_v reflection by the plane perpendicular to the x-y plane, needs to be used in order to transform one $\mathbf{R}$ in all others. By fitting the results of the tight-binding calculations to those from first-principle calculations [28], values of the following hopping integrals are obtained:

$$\begin{aligned} &E_{11}(\mathbf{R}_1) = t_0 = -0.184\text{ eV}, \quad E_{12}(\mathbf{R}_1) = t_1 = 0.401\text{ eV},\\ &E_{13}(\mathbf{R}_1) = t_2 = 0.507\text{ eV}, \quad E_{22}(\mathbf{R}_1) = t_{11} = 0.218\text{ eV},\\ &E_{23}(\mathbf{R}_1) = t_{12} = 0.338\text{ eV}, \quad E_{33}(\mathbf{R}_1) = t_{22} = 0.057\text{ eV}, \end{aligned} \tag{3}$$

while on-site energy of d_{z^2} is equal to $\varepsilon_0 = 1.046$ eV and of d_{xy} and $d_{x^2-y^2}$ is equal to $\varepsilon_2 = 2.104$ eV. Using values from Eqs. (2) and (3), the off-diagonal matrices are obtained as

$$h(\mathbf{R}_1) = \begin{bmatrix} t_0 & t_1 & t_2 \\ -t_1 & t_{11} & t_{12} \\ t_2 & -t_{12} & t_{22} \end{bmatrix} = h(\mathbf{R}_6)^T, \tag{4}$$

$$h(\mathbf{R}_2) = \begin{bmatrix} t_0 & \frac{1}{2}t_1 - \frac{\sqrt{3}}{2}t_2 & -\frac{\sqrt{3}}{2}t_1 - \frac{1}{2}t_2 \\ -\frac{1}{2}t_1 - \frac{\sqrt{3}}{2}t_2 & \frac{1}{4}t_{11} + \frac{3}{4}t_{22} & -\frac{\sqrt{3}}{4}t_{11} - t_{12} + \frac{\sqrt{3}}{4}t_{22} \\ \frac{\sqrt{3}}{2}t_1 - \frac{1}{2}t_2 & -\frac{\sqrt{3}}{4}t_{11} + t_{12} + \frac{\sqrt{3}}{4}t_{22} & \frac{3}{4}t_{11} + \frac{1}{4}t_{22} \end{bmatrix} = h(\mathbf{R}_4)^T, \tag{5}$$

$$h(\mathbf{R}_3) = \begin{bmatrix} t_0 & \frac{1}{2}t_1 + \frac{\sqrt{3}}{2}t_2 & \frac{\sqrt{3}}{2}t_1 - \frac{1}{2}t_2 \\ -\frac{1}{2}t_1 + \frac{\sqrt{3}}{2}t_2 & \frac{1}{4}t_{11} + \frac{3}{4}t_{22} & \frac{\sqrt{3}}{4}t_{11} - t_{12} - \frac{\sqrt{3}}{4}t_{22} \\ -\frac{\sqrt{3}}{2}t_1 - \frac{1}{2}t_2 & \frac{\sqrt{3}}{4}t_{11} + t_{12} - \frac{\sqrt{3}}{4}t_{22} & \frac{3}{4}t_{11} + \frac{1}{4}t_{22} \end{bmatrix} = h(\mathbf{R}_5)^T. \tag{6}$$

Finally, the diagonal submatrices, which take into account the on-site energies, external scalar potential, and spin-orbit coupling (SOC), have the form

$$h_D = \begin{bmatrix} \varepsilon_0 + V(x,y) & 0 & 0 \\ 0 & \varepsilon_2 + V(x,y) & \pm 2i \\ 0 & \mp 2i & \varepsilon_2 + V(x,y) \end{bmatrix}, \tag{7}$$

where off-diagonal terms take into account the SOC. Upper sign is for spin up and the lower for spin down. Thus, the Hamiltonian used for calculating the eigenstates of the system is of the form

$$H = \begin{bmatrix} h_D & \cdots & h(\mathbf{R}_n) \\ \vdots & \ddots & \vdots \\ h(\mathbf{R}_n)^\dagger & \cdots & h_D \end{bmatrix}, \tag{8}$$

where one row describes one atom in the layer, i.e., its connections with other atoms (off-diagonal terms), as well as its on-site energies and SOC (diagonal terms).

Finally, it should be noted that the theory presented here, although given for the example of MoS_2, is applicable to all transition metal dichalcogenides (e.g., WS_2, $MoSe_2$, WSe_2, etc.). The only difference is in the value of its parameters (lattice constant, on-site energies, and hopping energies), which means that the results obtained here should be applicable to other TMDs.

III. IMPACT OF ORBITAL ASYMMETRY ON ELECTRICAL PROPERTIES

The d_{xy} and $d_{x^2-y^2}$ orbitals, which contribute to hopping, are asymmetric in the Mo atom layer, giving us six different ways that the Mo atoms can be connected. Therefore, the

final Hamiltonian will depend on the relative position of those orbitals with respect to each other. Now we choose a coordinate system such that the orbital wave functions of d_{xy} and $d_{x^2-y^2}$ are not rotated with respect to it. Then, for convenience, we label the way one atom in the Mo layer is connected to some other neighboring atom, i.e., which hopping matrix [Eqs. (4)–(6)] is used for representing the connection in the Hamiltonian [Eq. (8)], as connection type 1,2, . . . ,6, where connection type n means that the neighboring atom is displaced from the specified atom by the vector $\mathbf{R}_n$ (see Fig. 1). As such, we always specify which atom is used as the origin, since labeling is done from the point of view of that atom. An essential assumption is that the coordinate system is chosen such that orbital wave functions are not rotated with respect to it. Otherwise, connection type n would not correspond to a displacement of atoms by vector $\mathbf{R}_n$ (e.g., if all orbitals in Fig. 1 were to be rotated by $\pi/3$, the connection between atom 0 and 1 would correspond to connection type 2).

Expanding on the above considerations, we conclude that by assuming a certain form for the orbital wave function (i.e., rotation by a certain angle) in a given coordinate system we can vary the connection between atoms, which allows us to create systems with the same shape, but different electronic properties. However, a simpler approach is to make the above assumption that wave functions are not rotated with respect to a given coordinate system and simply rotate the whole system. This second approach basically corresponds to transferring from one coordinate system, where the orbital wave functions are rotated, into a coordinate system where they are not. Thus, instead of rotating the coordinates we are rotating the system. Both approaches are valid and represent two sides of the same coin. Perhaps the simplest example of this is given in Fig. 2. As shown in Fig. 2 we have two systems of triangular shape, with one oriented upwards [Fig. 2(a)] and the other oriented downwards [Fig. 2(b)]. The connection type between the atoms is denoted with red numbers for the direction indicated (as mentioned above, this simply indicates the type of connection atom n sees towards atom m, where in this case $n < m$). Although superficially similar, the connection types between atoms are different and one system cannot be transformed into the other. This point is most easily shown if we compare their Hamiltonians. If, for simplicity, we label $h(\mathbf{R}_1) = h_1, \ldots, h(\mathbf{R}_6) = h_6$, then, as given by Eq. (8), the Hamilton matrices of the two system shown by Figs. 2(a) and 2(b) are, respectively:

$$H_1 = \begin{bmatrix} h_D & h_2 & h_1 \\ h_4 & h_D & h_3 \\ h_6 & h_5 & h_D \end{bmatrix}, \tag{9}$$

$$H_2 = \begin{bmatrix} h_D & h_1 & h_3 \\ h_6 & h_D & h_4 \\ h_5 & h_2 & h_D \end{bmatrix}, \tag{10}$$

where the row number corresponds to the atom number in Fig. 2. Comparing the two matrices, it is not possible to obtain one matrix from the other by using similarity transforms. Consequently, the eigenvalues, and thus the electrical properties, of the two systems will be different.

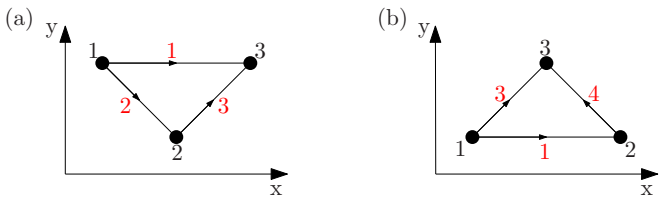

FIG. 2. (Color online) Two systems of three Mo atoms arranged in a triangle. Black dots represent atoms, while lines represent the connection between them. Atoms are labeled with black numbers, while connection types are labeled with red numbers. Connection type is for the direction indicated by the arrows.

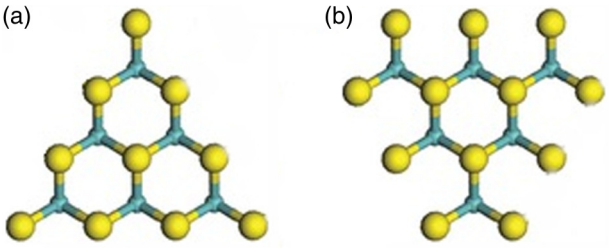

FIG. 3. (Color online) Two different triangular quantum dots with the same number of Mo atoms (blue balls). The S atoms are the yellow balls.

To make the above difference more clear, we show in Fig. 3 two different triangular quantum dots with the same number of Mo atoms. It should also be noted that surrounding S atoms are different for the two flakes. Although our calculations do not include the p orbitals, it is nonetheless important to indicate that the different physical arrangements of S atoms in the two systems could cause further differences in their electronic properties.

IV. TRIANGULAR QUANTUM DOTS

The first type of quantum dots that we will be exploring are equilateral triangular quantum dots, since they represent a natural extension of the discussion presented in the previous section. We will examine two triangular dots, one oriented upward (in positive direction of the y axis) as in Fig. 2(a) and one oriented downwards (in negative direction of the y axis) as in Fig. 2(b), with both systems containing the same number of atoms. We will refer to the former system as triangle up, and the latter as triangle down.

If the number of atoms at the edge of a quantum dot is N_E, then the total number of atoms in the system is given by

$$\frac{(N_E/3+2)(N_E/3+1)}{2}, \tag{11}$$

where, in order for a triangle to be equilateral, N_E must be divisible by 3. The calculations were done for $N_E = 48$. The considered systems are shown in Fig. 4. The obtained energy states for the two systems are shown in Fig. 5. Although monolayer MoS_2 has an energy band gap of 1.8 eV, in Fig. 5 we see that there are states inside this gap, which are due to the fact that we have finite systems. States found in the band gap are localized predominantly at the edges of the system

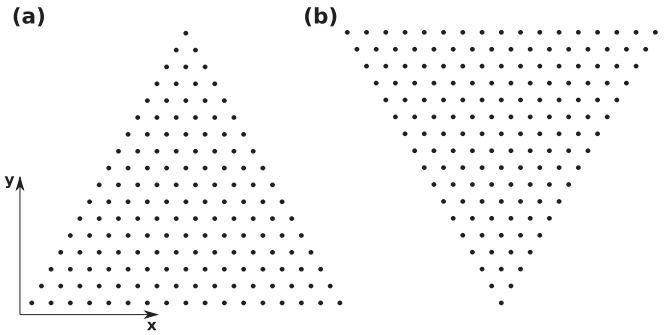

FIG. 4. The shape of two examined triangular quantum dots with the same dimensions and total number of atoms. The only difference is that the triangular dot (a) is oriented along the positive y direction (triangle up), and the dot (b) is oriented along the negative y direction (triangle down).

and are termed edge states. We also notice that the number of states in the valence band is lower than in the conduction band, which is a consequence of the fact that the valence band consists mainly of d_{z^2} orbitals, while the conduction band mainly consists of both d_{xy} and $d_{x^2-y^2}$ orbitals, resulting in more states. Furthermore, it can be concluded that energies obtained for spin up and spin down states in each system are the same, indicating that the SOC in the system has no effect on the obtained set of energies for different spins. This is in accordance with Kramer's degeneracy theorem, due to the absence of inversion symmetry in MoS_2 and the fact that states conduction and valence band are centered around opposite $\pm K$ points in the Brillouin zone. However, although the energies are the same, wave functions corresponding to those states are not necessarily the same. On the other hand, comparing the eigenenergies of the two systems, we see that the energy states are quite similar in the valence band up until the band gap (starting at 0 eV), while the difference is more noticeable in the conduction band (>1.8 eV). However, the greatest difference lies in the band gap area where edge states are found.

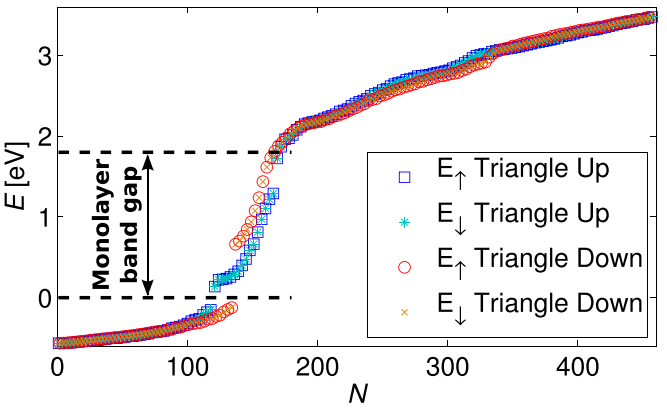

FIG. 5. (Color online) Energy states of two triangular quantum dots for $N_E = 48$, one oriented along the positive y axis (denoted as triangle up) and one oriented along the negative y axis (denoted as triangle down). Energies of both spin up and spin down states in each system are the same. The x axis numbers the states with increasing energy.

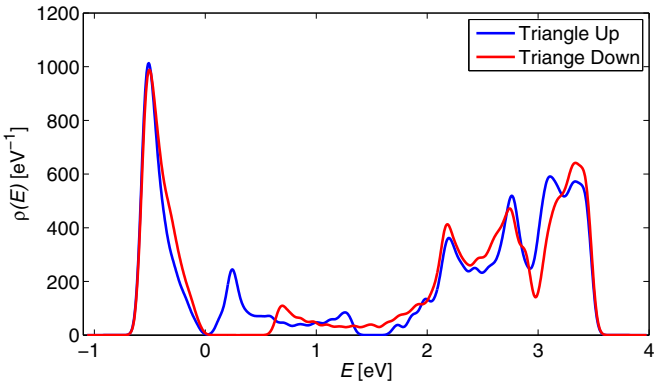

FIG. 6. (Color online) Total density of states corresponding to the system of Fig. 5. A broadening of 0.06 eV was used. Comparing the two systems, the density is quite similar in the valence band, somewhat different in the conduction band, and quite different in the band gap where edge states are found.

Similar conclusions can be obtained by examining the density of states, shown in Fig. 6. Here we introduced a Gaussian broadening of each energy level with width 0.06 eV. The DOS of the two systems are almost identical in the valence band up to the band gap. Difference in the conduction band is more noticeable because they are mostly made up of the asymmetric d_{xy} and $d_{x^2-y^2}$ orbitals, with both triangles exhibiting three peaks, but the magnitude and the width of those peaks are different. Finally, the difference is most noticeable in the area of the band gap, with the edge states in the triangle up localized closer to the valence band, while the edge states in the triangle up are localized closer to the conduction band.

The fact that edge states inside the band gap differ the most in both systems, lead us to the conclusion that the difference between the states in the valence and the conduction band are also due to states that are mainly localized at the edge of the system. Explanation for this can be found by first observing that the hexagonal system given in Fig. 1 is symmetric with respect to inversion about the y axis, i.e. "upper" and "lower" hexagon are identical. Having that in mind, we consider these two dots being constructed from these small hexagons, where those in the center are complete, while those at the edges are incomplete (part of them is cut off). Thus, the central part of both systems is symmetric with respect to inversion about the y axis and has the same electrical properties, while parts at the edge are not completely symmetric and therefore have different electrical properties. Examples of this are shown in Fig. 7. Local density of states (LDOS) for states shown in Figs. 7(a) and 7(b) is similar. Since they are both localized at the center of their respective systems, they have similar energy. On the other hand, states shown in Figs. 7(c) and 7(d) also have similar LDOS distribution, but are localized more at the edges of the system and therefore the difference in energy is quite noticeable.

V. HEXAGONAL QUANTUM DOTS

Now we explore the electronic properties of hexagonal quantum dots which have a higher symmetry than the previous triangular quantum dots and which are more unique in

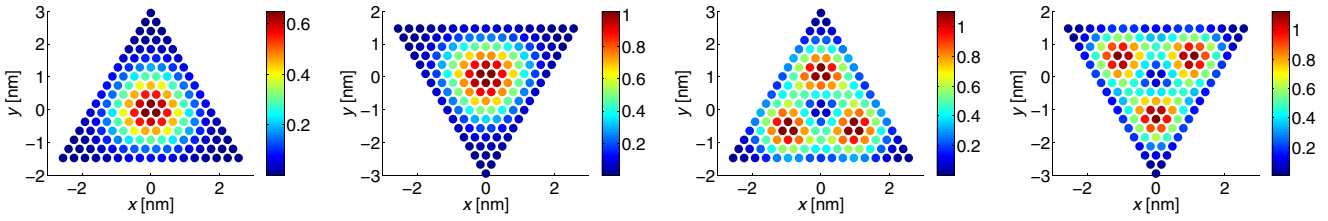

(a) $E = -0.087$ eV (b) $E = -0.088$ eV (c) $E = -0.178$ eV (d) $E = -0.125$ eV

FIG. 7. (Color online) Local density of states (LDOS) for states in the valence band of triangle up and triangle down quantum dots with similar LDOS distribution. Since states with similar LDOS (and thus wave function) shown in (a) and (b) are localized at the center of the dot, the difference in their energies is minor (∼1 meV), while the difference between states with similar distribution shown in (c) and (d) is larger (∼50 meV) since they are localized closer to the edges.

their edge termination. Furthermore, using this geometry of nanoflake as a basis, the effect of system size on the density of edge states will be explored.

If we denote the number of atoms at the edge of a hexagonal nanoflake as N_E, then the total number of atoms in the dot is given by

$$3\left(\frac{N_E-6}{6}\right)^2+9\,\frac{N_E-6}{6}+7, \tag{12}$$

where, in order for a dot to be equilateral, N_E must be divisible by six. We consider first a dot with $N_E = 48$. Energy states obtained for the system are shown in Fig. 8. Similarly to the case for triangular quantum dots, energies for both spin up and spin down are the same and there are fewer states in the valence band than in the conduction band, since the majority of states in the conduction band is made from combinations of d_{xy} and $d_{x^2-y^2}$ orbitals, and the majority of states in the valence band originate from d_{z^2} orbitals, giving us almost twice the number of states. Notice that edge states are almost uniformly distributed across the band gap.

The total density of states (DOS) plot is given in Fig. 9. Notice that there are three peaks in the conduction band DOS. These peaks are located close to 2.2, 2.8, and 3.4 eV. On the other hand, in the valence band the majority of states is located in the center of the band, around −0.5 eV. This distribution of states in the two bands can be linked to the position of local minima in the energy spectrum of bulk monolayer MoS_2. Notice that the edge states are rather evenly distributed across the band gap, with somewhat more states located closer to the edge of the valence band.

Finally, we examine the effect of the dot size on the DOS, and in particular the edge states within the band gap. The calculations were done for values of $N_E = 6$–132, where the DOS for $N_E = 132$ approaches the bulk result. Normalized DOS for different system sizes is shown in Fig. 10. Only results for spin up are shown, since, as discussed previously, the results for spin down are the same. Looking at Fig. 10, we notice that for small N_E (<30), the states are localized around certain energies, especially noticeable in the band gap and somewhat less in the conduction and the valence bands. This is due to the fact that these systems are relatively small and quantization effects are pronounced. We also see that in those cases, the DOS of the edge states in the band gap has a comparable strength to the DOS in the conduction and the valence band. Examining the DOS for larger N_E (>30) leads us to conclude that the overall form of the density of states in both the conduction and the valence band remains similar (notice that the DOS from $N_E = 96$ to $N_E = 132$ is almost indistinguishable) and overall increases as N_E increases, as expected. On the other hand, examining the band gap, we see that the rate with which the DOS increases in that area is a lot smaller. This leads us to the conclusion that as the size of the system increases the percentage of states that reside inside

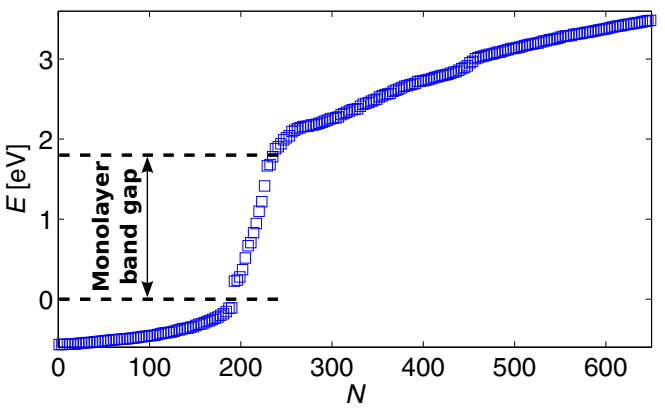

FIG. 8. (Color online) Energy states of a hexagonal quantum dot with $N_E = 48$. Notice the appearance of edge states within the bulk band gap (0–1.8 eV). The x axis numbers the states with increasing energy.

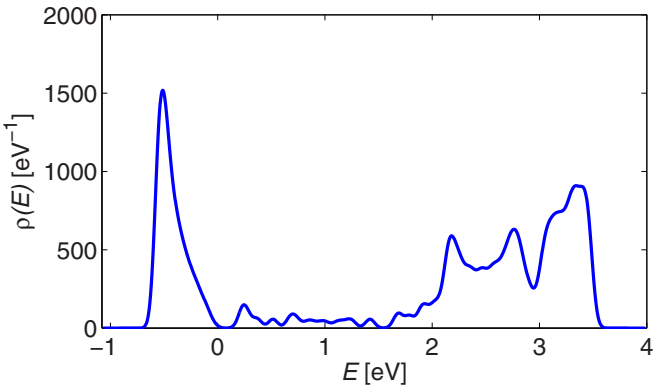

FIG. 9. (Color online) Density of states (DOS) for the hexagonal dot of Fig. 8.

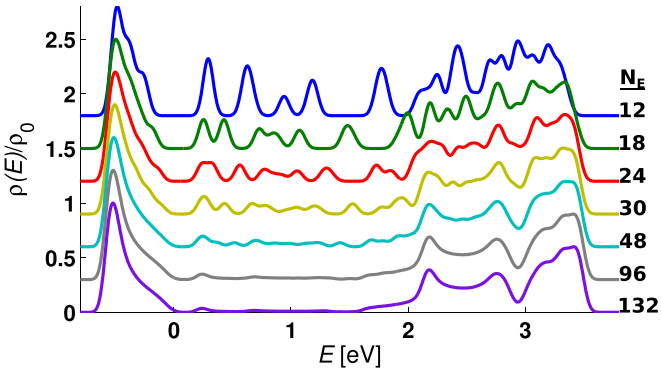

FIG. 10. (Color online) Normalized density of states (DOS) for different sizes of the hexagonal dot measured by the number of atoms at the edge of a system N_E. For clarity we displaced the different curves in the vertical direction.

the band gap decreases. This behavior is in accordance with the expectation that with increasing the size of the system, the relative number of edge states decreases.

VI. CONCLUDING REMARKS

Electronic properties of molybdenum disulfide, MoS_2, triangular and hexagonal quantum dots were calculated within the tight-binding model. Using the nearest neighbor approximation and first-principle calculations show that the valence and the conduction band are made mostly from d_{z^2}, d_{xy}, and $d_{x^2-y^2}$ orbitals. The hopping matrices and Hamiltonian used for the calculations were derived. It is shown that the asymmetry of the d_{xy} and $d_{x^2-y^2}$ orbitals in the plane of Mo atoms enables us to form quantum dots of the same shape but with different electrical properties. This is first demonstrated on a simple system and then further investigated for the case of two triangular quantum dots. It is shown that systems differ mostly in areas around the edges explaining why the largest difference in energies is between states localized at the edges of the system, most notably the edge states in the band gap. It should be noted that observed difference in properties that stem primarily from edge states is not specific only to the MoS_2 or TMDs in general and that similar behavior was reported in graphene [29,30], where different magnetic properties were observed for differently shaped graphene nanoislands stemming mostly from states localized at the edges of the system.

The energy spectrum and density of states (DOS) of triangular and hexagonal quantum dots were investigated. We concluded that edge states appear in the area of the bulk band gap (0–1.8 eV) due to the finiteness of the system. We also found that there are more states in the conduction than in the valence band, as well as that there are a number of peaks in the conduction band which correspond to local minima found in the bulk monolayer conduction band.

The effect of system size on the DOS was investigated. We showed that for sufficiently large systems, the shape of the DOS in the conduction and valence band remains similar and that the percentage of states that reside inside the band gap decreases, in accordance with expectations.

Finally, as previously mentioned, the tight-binding method used in our calculations is applicable to other TMDs and as such, the general conclusions obtained in this work should be applicable to many different TMD (e.g., WS_2, $MoSe_2$, WSe_2, etc.) flakes.

ACKNOWLEDGMENTS

This work was supported by the Flemish Science Foundation (FWO-Vl) and the Methusalem Foundation of the Flemish government. Stefan Pavlović is supported by JoinEU-SEE IV, Erasmus Mundus Action 2 programme. We thank J. M. Pereira for interesting discussions.

[1] K. F. Mak, C. Lee, J. Hone, J. Shan, and T. F. Heinz, Phys. Rev. Lett. **105**, 136805 (2010).
[2] A. Splendiani, L. Sun, Y. Zhang, T. Li, J. Kim, C.-Y. Chim, G. Galli, and F. Wang, Nano Lett. **10**, 1271 (2010).
[3] S. Tongay, J. Zhou, C. Ataca, K. Lo, T. S. Matthews, J. Li, J. C. Grossman, and J. Wu, Nano Lett. **12**, 5576 (2012).
[4] J. S. Ross, S. Wu, H. Yu, N. Ghimire, A. Jones, G. Aivazian, J. Yan, D. Mandrus, D. Xiao, W. Yao, and X. Xu, Nat. Commun. **4**, 1474 (2013).
[5] H. Zeng, G.-B. Liu, J. Dai, Y. Yan, B. Zhu, R. He, L. Xie, S. Xu, X. Chen, W. Yao, and X. Cui, Sci. Rep. **3**, 1608 (2013).
[6] B. Radisavljevic, A. Radenovic, J. Brivio, V. Giacometti, and A. Kis, Nat. Nanotechnol. **6**, 147 (2011).
[7] D. Lembke and A. Kis, ACS Nano **6**, 10070 (2012).
[8] M.-W. Lin, L. Liu, Q. Lan, X. Tan, K. S. Dhindsa, P. Zeng, V. M. Naik, M. M.-C. Cheng, and Z. Zhou, J. Phys. D **45**, 345102 (2012).
[9] W. Bao, X. Cai, D. Kim, K. Sridhara, and M. S. Fuhrer, Appl. Phys. Lett. **102**, 042104 (2013).
[10] S. Larentis, B. Fallahazad, and E. Tutuc, Appl. Phys. Lett. **101**, 223104 (2012).
[11] H. Fang, S. Chuang, T. C. Chang, K. Takei, T. Takahashi, and A. Javey, Nano Lett. **12**, 3788 (2012).
[12] D. Xiao, W. Yao, and Q. Niu, Phys. Rev. Lett. **99**, 236809 (2007).
[13] W. Yao, D. Xiao, and Q. Niu, Phys. Rev. B **77**, 235406 (2008).
[14] O. Gunawan, Y. P. Shkolnikov, K. Vakili, T. Gokmen, E. P. De Poortere, and M. Shayegan, Phys. Rev. Lett. **97**, 186404 (2006).
[15] A. Rycerz, J. Tworzydlo, and C. W. J. Beenakker, Nat. Phys. **3**, 172 (2007).
[16] Z. Zhu, A. Collaudin, B. F. W. Kang, and K. Behnia, Nat. Phys. **8**, 89 (2012).
[17] D. Xiao, G.-B. Liu, W. Feng, X. Xu, and W. Yao, Phys. Rev. Lett. **108**, 196802 (2012).
[18] H. Zeng, J. Dai, W. Yao, D. Xiao, and X. Cui, Nat. Nanotechnol. **7**, 490 (2012).
[19] H. Terrones, F. López-Urías, and M. Terrones, Sci. Rep. **3**, 1549 (2013).
[20] A. Kormányos, V. Zólyomi, N. D. Drummond, and G. Burkard, Phys. Rev. X **4**, 011034 (2014).
[21] G.-B. Liu, H. Pang, Y. Yao, and W. Yao, New J. Phys. **16**, 105011 (2014).

[22] R. A. Bromley, R. B. Murray, and A. D. Yoffe, J. Phys. C **5**, 759 (1972).
[23] L. F. Mattheiss, Phys. Rev. B **8**, 3719 (1973).
[24] Z. Y. Zhu, Y. C. Cheng, and U. Schwingenschlögl, Phys. Rev. B **84**, 153402 (2011).
[25] E. S. Kadantsev and P. Hawrylak, Solid State Commun. **152**, 909 (2012).
[26] S. Lebègue and O. Eriksson, Phys. Rev. B **79**, 115409 (2009).
[27] C. Ataca, H. Sahin, and S. Ciraci, J. Phys. Chem. C **116**, 8983 (2012).
[28] G.-B. Liu, W.-Y. Shan, Y. Yao, W. Yao, and D. Xiao, Phys. Rev. B **88**, 085433 (2013).
[29] J. Fernandez-Rossier and J. J. Palacios, Phys. Rev. Lett. **99**, 177204 (2007).
[30] Z. Z. Zhang, K. Chang, and F. M. Peeters, Phys. Rev. B **77**, 235411 (2008).